Use of a Network Simulation Method for the Determination of the Response of a Colloidal Suspension to a Constant Electric Field

ARTICLE *in* THE JOURNAL OF PHYSICAL CHEMISTRY B · DECEMBER 1999

Impact Factor: 3.3 · DOI: 10.1021/jp991521f

4 AUTHORS:

José Juan López-García
Universidad de Jaén
18 PUBLICATIONS **279** CITATIONS
SEE PROFILE

Jose Horno
Universidad de Jaén
68 PUBLICATIONS **896** CITATIONS
SEE PROFILE

Angel V Delgado
University of Granada
225 PUBLICATIONS **4,115** CITATIONS
SEE PROFILE

Fernando González-Caballero
University of Granada
146 PUBLICATIONS **2,637** CITATIONS
SEE PROFILE

Use of a Network Simulation Method for the Determination of the Response of a Colloidal Suspension to a Constant Electric Field

J. J. López-García,[†] J. Horno,*[,†] A. V. Delgado,[‡] and F. González-Caballero[‡]

Departamento de Física, Facultad de Ciencias Experimentales, Universidad de Jaén, Paraje Las Lagunillas s/n, 23071 Jaén, Spain, and Departamento de Física Aplicada, Facultad de Ciencias, Universidad de Granada, 18071 Granada, Spain

Received: May 7, 1999; In Final Form: July 26, 1999

A network simulation method, based on the theory of network thermodynamics, is applied in this work to the description of the structure of the double layer around a spherical colloidal particle, in the presence of an externally applied constant electric field. It is demonstrated that the system of differential equations governing the phenomena involved is formally equivalent to that of a properly designed electric circuit, obtained as a series of subcircuits corresponding to each of the volume elements into which the system is divided. A simulation program is then used to solve the circuit in order to obtain the quantities of interest. The methodology is first applied to the calculation of the electrophoretic mobility of a spherical colloidal particle, and of the dc conductivity of a dilute suspension of spheres. The results are compared to the predictions of O'Brien and White's classical theories, and an excellent agreement is found in all cases checked. We emphasize that the network technique not only avoids the knowledge of sophisticated numerical integration methods but also allows one to readily obtain the profiles of any physical variable of interest (potential, ionic concentrations, fluid velocity, for instance) at all points of the double layer. The polarization of the latter under the action of the applied external field is easily described in terms of the dependence of the variables with the distance to the particle's surface. The power of the method is illustrated by the calculation of ion concentrations, and potential and velocity profiles in the presence of the external electric field.

Introduction

It is well-known that the body of differential equations governing the response of a colloidal system to a constant external electric field cannot be analytically solved but for a limited number of cases, restricted to low values of the electrokinetic or zeta potential (ζ), small thickness of the electric double layer, etc.[1−5] The solution of the problem in the general case requires the use of numerical methods,[6,7] among which the computation procedures devised by O'Brien and White[7] for electrophoresis, or by O'Brien for dc conductivity,[8] have become classical. Nevertheless, approximate methods have the advantage that illustrate the physical phenomena involved better than computational ones. Information about such questions as how are the ionic concentrations influenced by the field, or what is the geometry of the velocity profile of liquid around the particle, is somewhat hidden in the numerical routines.

In this work, we propose a different approach to the calculation of such quantities as the electrophoretic mobility of a colloidal sphere, or the electrical conductivity of a suspension. We show that, while the method can achieve an accuracy comparable to that of the best numerical routines, it readily provides answers to the questions mentioned above. We call this procedure a network simulation method, since it is based on the theory of network thermodynamics,[9,10] in which basically the flux−force relationships in dynamical systems are described in terms of electric networks. Network thermodynamics takes advantage of the formal similarities between the mathematical structure underlying different phenomena with the same balance and constitutive equations. In short, the target is to find an electric circuit that possesses the same balance and constitutive equations as the physical problem of interest.

The latter is thus reduced to solve (i.e., to find currents and voltages in properly chosen branches and nodes) the circuit; the interesting point is that there is highly developed commercially available software for circuit analysis that can be employed to simulate the behavior of the circuit. In this way, the physical problem can be solved without having to deal with the solution of the governing differential equations. Furthermore, the voltages and currents in different parts of the network will provide information about the spatial dependence of the variables of interest (electric potential, fluid velocity, and so on).

The method has been successfully applied to a variety of problems, including ionic transport in both membranes[11] and electrochemical cells,[12] coupled chemical−electrochemical reactions at a planar electrode,[13,14] or the calculation of the potential distribution in the electric double layer around a colloid particle.[15]

In this work, our aim is to show the capabilities of the method in computing the electrophoretic mobility and the dc conductivity in colloidal suspensions, as well as in providing a detailed account of how any of the other quantities of interest in the polarized double layer differ, under the action of the external field, from their equilibrium values.

Mathematical Description of the Problem

We consider first a single spherical particle immersed in a general electrolyte solution of viscosity η and permittivity ϵ_{ext}, composed of N ionic species, with valencies z_i, diffusion

* Corresponding author. E-mail: jhorno@ujaen.es.
[†] Universidad de Jaén.
[‡] Universidad de Granada.

10.1021/jp991521f CCC: $18.00
Published on Web 12/03/1999

coefficients D_i, and bulk concentrations c_i^∞ ($i = 1, ..., N$). The equations governing the dynamics of this system are well-known:

(a) Nernst−Planck equations:

$$\vec{J}_i(\vec{r}) = -D_i\nabla c_i(\vec{r}) - \frac{z_i e D_i}{kT} c_i(\vec{r})\nabla\phi(\vec{r}) + c_i(\vec{r})\vec{v}(\vec{r}) \qquad (i = 1, ..., N) \quad (1)$$

(b) ionic conservation:

$$\nabla\cdot\vec{J}_i(\vec{r}) = 0 \qquad (i = 1, ..., N) \quad (2)$$

(c) Poisson equation:

$$\nabla^2\phi(\vec{r}) = -\frac{eN_A\sum_{i=1}^{N} z_i c_i(\vec{r})}{\epsilon_{ext}} \quad (3)$$

(d) Navier−Stokes equation:

$$\eta\nabla^2\vec{v}(\vec{r}) - \nabla P(\vec{r}) = eN_A\left(\sum_{i=1}^{N} z_i c_i(\vec{r})\right)\nabla\phi(\vec{r}) + \rho_f(\vec{v}(\vec{r})\cdot\nabla)\vec{v}(\vec{r}) \quad (4)$$

(e) fluid incompressibility:

$$\nabla\cdot\vec{v}(\vec{r}) = 0 \quad (5)$$

where ϕ is the electric potential, $\vec{v}$ is the fluid velocity, P is the pressure, ρ_f is the density of the dispersion medium, and other symbols have their usual meanings.

Upon application of an external electric field, all variables are perturbed about their spherically symmetric equilibrium values (denoted by the superscript "0" in what follows):

$$c_i(\vec{r}) = c_i^0(r) + \delta c_i(\vec{r}) \quad (6)$$

$$\phi(\vec{r}) = \phi^0(r) + \delta\phi(\vec{r}) \quad (7)$$

Assuming that the z-axis of the reference system, centered in the particle, is in the direction of the field, and that the latter is low enough for the vector quantities of the problem to be linear in the field, it is possible to write

$$\vec{J}_i(\vec{r}) = J_{ir}(r)\cos\theta\,\mathbf{e}_r + J_{i\theta}(r)\sin\theta\,\mathbf{e}_\theta \quad (8)$$

$$\vec{v}(\vec{r}) = v_r(r)\cos\theta\,\mathbf{e}_r + v_\theta(r)\sin\theta\,\mathbf{e}_\theta \quad (9)$$

From eq 9, the vorticity $\vec{\Omega}(\vec{r}) = \nabla\times\vec{v}(\vec{r})$ will read

$$\vec{\Omega}(\vec{r}) = \Omega(r)\sin\theta\,\mathbf{e}_\varphi \quad (10)$$

In these equations, $\mathbf{e}_r$, $\mathbf{e}_\theta$, $\mathbf{e}_\varphi$ are the unit vectors in spherical coordinates. Similarly, the perturbations in concentration or potential must be

$$\delta c_i(\vec{r}) = \delta c_i(r)\cos\theta$$
$$\delta\phi(\vec{r}) = \delta\phi(r)\cos\theta \quad (11)$$

For computational reasons, it is convenient to use the dimensionless variables

$$\delta y(r) = \frac{e\delta\phi(r)a}{kTr} \quad (12)$$

$$n_i(r) = \frac{a}{r}\left(\frac{\delta c_i(r)}{c_i^0(r)} + \frac{z_i e\delta\phi(r)}{kT}\right) \quad (13)$$

$$u_r(r) = \frac{ae^2\eta}{(kT)^2\epsilon_{ext}}(v_r(r) - v_r(r\rightarrow\infty)) \quad (14)$$

$$\omega(r) = \frac{a^2e^2\eta\Omega(r)}{(kT)^2\epsilon_{ext}} \quad (15)$$

$$y^0(r) = \frac{e\phi^0(r)}{kT} \quad (16)$$

$$\xi = \frac{a}{r} \quad (17)$$

where a is the radius of the slipping plane.

Using these variables, and keeping only linear terms in the perturbed quantities, Nernst−Planck, Poisson, and Navier−Stokes equations lead to

$$\frac{\partial^2 n_i(\xi)}{\partial\xi^2} = \frac{2}{\xi}\frac{\partial n_i(\xi)}{\partial\xi} + z_i\frac{dy^0(\xi)}{d\xi}\left[\frac{\partial n_i(\xi)}{\partial\xi} - \frac{n_i(\xi)}{\xi} + \frac{(kT)^2\epsilon_{ext}}{e^2\eta D_i\xi}(u_r(\xi) - u_r(\xi=1))\right] \quad (18)$$

$$\frac{\partial^2\delta y(\xi)}{\partial\xi^2} = \frac{2}{\xi}\frac{\partial\delta y(\xi)}{\partial\xi} - \frac{(\kappa a)^2}{\xi^4\sum_{i=1}^{N} z_i^2 c_i^\infty}\sum_{i=1}^{N} z_i c_i^0(\xi)(n_i(\xi) - z_i\delta y(\xi)) \quad (19)$$

$$\frac{\partial^2 u_r(\xi)}{\partial\xi^2} = \frac{2}{\xi}\frac{\partial u_r(\xi)}{\partial\xi} - \frac{2\omega(\xi)}{\xi^3} \quad (20)$$

$$\frac{\partial^2\omega(\xi)}{\partial\xi^2} = \frac{2\omega(\xi)}{\xi^2} - \frac{(\kappa a)^2}{\xi^2\sum_{i=1}^{N} z_i^2 c_i^\infty}\sum_{i=1}^{N} z_i c_i^0(\xi)\frac{dy^0(\xi)}{d\xi}n_i(\xi) \quad (21)$$

where κ represents the reciprocal Debye length:

$$\kappa = \sqrt{\frac{e^2N_A\sum_{i=1}^{N} z_i^2 c_i^\infty}{kT\epsilon_{ext}}} \quad (22)$$

Note that eqs 18, 20, and 21 are independent of δy, and hence the electrophoretic mobility will not depend on the electrostatic boundary conditions, as demonstrated by O'Brien and White.[7]

The boundary conditions for the electrophoretic problem have been widely described;[1,3−7] hence only a brief account will be given, in terms of the dimensionless variables chosen in this work. Thus, the equilibrium electric potential must equal ζ, the

electrokinetic potential at $r = a$, and tend to zero far from the particle:

$$y^0(\xi=1) = \frac{e\zeta}{kT}; \quad y^0(\xi=0) = 0 \tag{23}$$

whereas double layer effects must be negligible for large r:

$$\frac{\partial \delta\phi(r)}{\partial r}|_{r\to\infty} \to -E_a$$

$$\delta c_i(r\to\infty) \to 0 \qquad (i = 1, ..., N) \tag{24}$$

E_a being the strength of the external field. From these equations, the dimensionless variables δy (eq 12) and n_i (eq 13) must fulfill the conditions:

$$\delta y(\xi=0) = -\frac{eE_a a}{kT} = -\beta \tag{25}$$

$$n_i(\xi=0) = -\frac{z_i eE_a a}{kT} = -z_i\beta \qquad (i = 1, ..., N) \tag{26}$$

In addition, it will be assumed that ions and liquid behind the slipping plane are immobile (the so-called classical or standard electrokinetic model). Hence, the normal components of ion fluxes must vanish at $r = a$, whereby

$$\frac{\partial n_i}{\partial \xi}|_{\xi=1} = n_i(\xi=1) \qquad (i = 1, ..., N) \tag{27}$$

On the other hand, the boundary condition for δy on the particle is obtained from the continuity of the electric displacement vector and can be written as

$$\frac{\partial \delta y(\xi)}{\partial \xi}|_{\xi=1} = \frac{\epsilon_{ext} - \epsilon_{int}}{\epsilon_{ext}}\delta y(\xi=1) \tag{28}$$

where ϵ_{int} is the permittivity of the particle.

Boundary conditions for the fluid velocity and vorticity are also needed. The requisite that the velocity vanishes at $r = a$ (nonslip condition), together with the incompressibility of the liquid lead to

$$\frac{\partial u_r}{\partial \xi}|_{\xi=1} = 0; \quad u_r(\xi=0) = 0 \tag{29}$$

Obtaining the boundary conditions for the vorticity is somewhat more involved. Far from the particle it must be negligible:

$$\omega(\xi=0) = 0 \tag{30}$$

The condition on the slipping plane requires considering the force balance on the particle: in the steady state, the total force, resulting from the sum of the electric ($\vec{F}_e$) and viscous ($\vec{F}_v$) contributions must vanish. The latter is given by[7]

$$\vec{F}_v = -\frac{4}{3}\pi a^2(P(r=a) + 2\eta\Omega(r=a)) \tag{31}$$

Using Navier−Stokes equation, (31) can be written as

$$\vec{F}_v = -\frac{4}{3}\pi a^2\left(-eN_A\sum_{i=1}^{N} z_i c_i^0(r=a)\delta\phi(r=a) - \eta a\frac{\partial\Omega(r)}{\partial r}\Big|_{r=a} + \eta\Omega(r=a)\right) \tag{32}$$

The electric force on the particle must be equal and opposite to that on the ions in the double layer:

$$\vec{F}_e = eN_a\int_V\sum_{i=1}^{N} z_i c_i(\vec{r})\nabla\phi(\vec{r})\,dV \tag{33}$$

where V is a volume enclosing the particle and its double layer. Since $\vec{F}_e + \vec{F}_v = 0$

$$\frac{\partial\omega(\xi)}{\partial\xi}|_{\xi=1} = (\kappa a)^2\int_1^0\sum_{i=1}^{N} z_i\frac{dy^0(\xi)}{d\xi}c_i^0(\xi)\frac{n_i(\xi)}{\xi^3}d\xi - \omega(\xi=1) \tag{34}$$

that constitutes the boundary condition for the vorticity on the particle surface ($\xi = 1$).

Network Model

We now proceed to design an electric circuit equivalent to the physical problem in hand, that is, with the same governing differential equations. The method involves dividing the physical region of interest (the particle and its double layer) into N_c compartments or volume elements small enough for spatial variations to be negligible within each compartment. Since the network model of the equilibrium Poisson−Boltzmann equation has been discussed elsewhere,[15] we will focus on the nonequilibrium situation. Thus, the Nernst−Planck equations (1) can be written in the form

$$\frac{\partial h_i(\xi)}{\partial\xi} = -\frac{2}{\xi}\frac{\partial n_i(\xi)}{\partial\xi} - z_i\frac{dy^0(\xi)}{d\xi}\left[\frac{\partial n_i(\xi)}{\partial\xi} - \frac{n_i(\xi)}{\xi} + \frac{(kT)^2\epsilon_{ext}}{e^2 D_i\eta\xi}(u_r(\xi) - u_r(\xi=1))\right] \tag{35}$$

with

$$h_i(\xi) = -\frac{\partial n_i(\xi)}{\partial\xi} \tag{36}$$

Equation 36 can be easily discretized

$$h_i\left(\xi_j \pm \frac{\Delta\xi_j}{2}\right) = \pm\frac{n_i(\xi_j) - n_i\left(\xi_j \pm \frac{\Delta\xi_j}{2}\right)}{\frac{\Delta\xi_j}{2}} \tag{37}$$

formally identical to Ohm's law if n_i plays the role of the voltage, h_i the current, and $\Delta\xi_j/2$ the resistance.

Similarly, the discretized version of eq 35 would indicate that the currents $h_i(\xi_j + \Delta\xi_j/2)$ and $h_i(\xi_j - \Delta\xi_j/2)$ differ because of the presence of a current source G_{ij} with strength:

$$G_{ij} = -\left[\frac{z_i}{\Delta\xi}\left(y^0\left(\xi_j + \frac{\Delta\xi_j}{2}\right) - y^0\left(\xi_j - \frac{\Delta\xi_j}{2}\right)\right) + \frac{2}{\xi_j}\right] \times \left[n_i\left(\xi_j + \frac{\Delta\xi_j}{2}\right) - n_i\left(\xi_j - \frac{\Delta\xi_j}{2}\right)\right] + \frac{z_i}{\xi_j}\left(y^0\left(\xi_j + \frac{\Delta\xi_j}{2}\right) - y^0\left(\xi_j - \frac{\Delta\xi_j}{2}\right)\right)n_i(\xi_j) - \frac{z_i}{\xi_j}\left(y^0\left(\xi_j + \frac{\Delta\xi_j}{2}\right) - y^0\left(\xi_j - \frac{\Delta\xi_j}{2}\right)\right) \times \frac{(kT)^2\epsilon_{\text{ext}}}{e^2 D_i \eta}(u_r(\xi_j) - u_r(\xi{=}1)) \quad (38)$$

as shown schematically in Figure 1a.

A similar procedure is followed with the potential variation by defining

$$h(\xi) = -\frac{\partial \delta y(\xi)}{\partial \xi} \quad (39)$$

which can be discretized to take the form of Ohm's law with δy as voltage, h as current, and $\Delta\xi_j/2$ as resistance.

Using eq 39, the Poisson equation for the potential variation (19) can be interpreted by saying that the currents $h(\xi_j + \Delta\xi_j/2)$ and $h(\xi_j - \Delta\xi_j/2)$ differ because of the presence of a current source GP_j with strength:

$$GP_j = -\frac{2}{\xi_j}\left[\delta y\left(\xi_j + \frac{\Delta\xi_j}{2}\right) - \delta y\left(\xi_j - \frac{\Delta\xi_j}{2}\right)\right] + \frac{(\kappa a)^2 \Delta\xi_j \sum_{i=1}^{N} z_i c_i^0(\xi_j)(n_i(\xi_j) - z_i \delta y(\xi_j))}{\xi_j^4 \sum_{i=1}^{N} z_i^2 c_i^\infty} \quad (40)$$

as depicted in Figure 1b.

For the network representation of the vorticity, we define

$$h_\omega(\xi) = -\frac{\partial \omega(\xi)}{\partial \xi} \quad (41)$$

that can be discretized as describe above. Also using eq 41, the vorticity eq 21 can be interpreted by saying that the currents $h_\omega(\xi_j + \Delta\xi_j/2)$ and $h_\omega(\xi_j - \Delta\xi_j/2)$ differ because of the presence of a resistor $\xi_j^2/(2\Delta\xi_j)$ between the node ξ_j and earth, and a current source $G\omega_j$

$$G\omega_j = \frac{(\kappa a)^2}{\xi_j^2 \sum_{i=1}^{N} z_i^2 c_i^\infty} \sum_{i=1}^{N} z_i c_i^0(\xi_j)\left[y^0\left(\xi_j + \frac{\Delta\xi_j}{2}\right) - y^0\left(\xi_j - \frac{\Delta\xi_j}{2}\right)\right] n_i(\xi_j) \quad (42)$$

as depicted in Figure 1c.

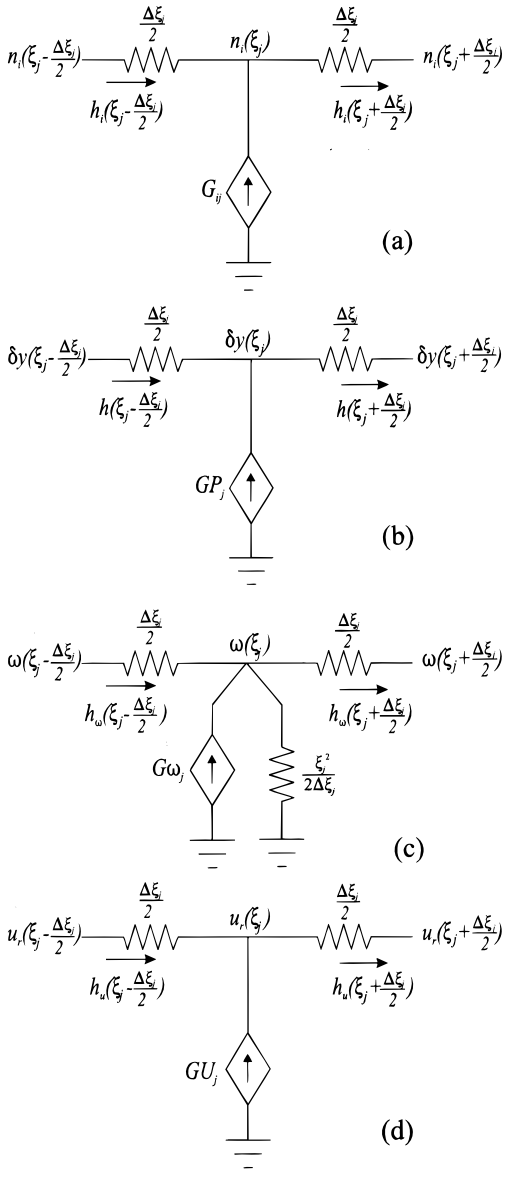

Figure 1. (a) Network model of the discretized Nernst−Planck equation for ionic species i in compartment j. (b) Same as (a) for the Poisson equation. (c) Same as (a) for the vorticity. (d) Same as (a) for the radial component of the velocity.

Finally, we seek to obtain the network model for the radial component of the velocity. As before, we define

$$h_u = -\frac{\partial u_r(\xi)}{\partial \xi} \quad (43)$$

that can be discretized as described above. From this, the differential eq 20 is equivalent to the circuit of Figure 1d, where a current source

$$GU_j = \frac{2\Delta\xi_j}{\xi_j^3}\omega(\xi_j) - \frac{2}{\xi_j}\left[u_r\left(\xi_j + \frac{\Delta\xi_j}{2}\right) - u_r\left(\xi_j - \frac{\Delta\xi_j}{2}\right)\right] \quad (44)$$

is used to account for the differences between the currents h_u-$(\xi_j + \Delta\xi_j/2)$ and $h_u(\xi_j - \Delta\xi_j/2)$.

All the effects just described can be put together by connecting several subcircuits, as illustrated in Figure 2. N_c of such subcircuits ($j = 1, ..., N_c$) must be connected in series to yield a network model of the transport processes in the entire

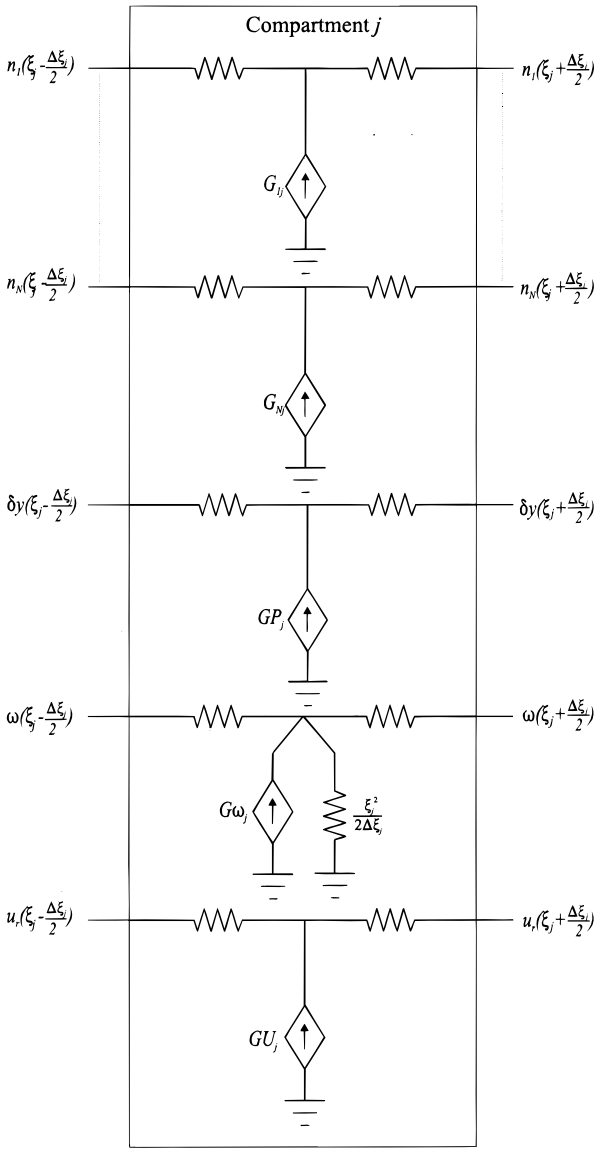

Figure 2. Network model for the *j*th compartment for the transport processes in a dilute colloidal suspension under the action of a constant electric field.

physical region. Inclusion of the boundary conditions will be described below.

The conditions (25) and (28) can be modeled by means of an independent voltage source $-\beta$ at $\xi = 0$, and a resistor of value $R = \epsilon_{ext}/(\epsilon_{int} - \epsilon_{ext})$ between earth and the node $\xi = 1$, respectively. Similarly, the conditions (26) and (27) can be modeled as an independent voltage source $-z_i\beta$ at $\xi = 0$, and a resistor of value $R_i = -1$ between earth and the node $\xi = 1$, respectively. Concerning the boundary conditions for the vorticity, they can be included in the circuit by earthing the node $\xi = 0$, and connecting at $\xi = 1$ a resistor of value 1 and a current source

$$GBS = (\kappa a)^2 \int_0^1 \sum_{i=1}^{N} z_i \frac{dy^0(\xi)}{d\xi} c_i^0(\xi) \frac{n_i(\xi)}{\xi^3} d\xi \qquad (45)$$

Finally, the boundary conditions for the radial component of the fluid velocity will be implemented by connecting to earth the node $\xi = 0$, and inserting a independent current source of zero intensity at $\xi = 1$.

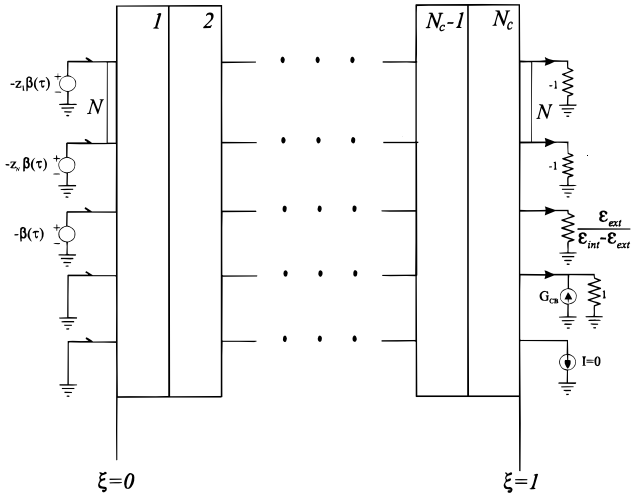

Figure 3. Global network model for the transport in a dilute colloidal suspension under the action of a constant electric field. The system is divided into N_c compartments such as those in Figure 2, with N_c = 300.

With all this information, the global network model for the ionic transport in a dilute colloidal suspension can be obtained as sketched in Figure 3.

Using the Circuit To Obtain Physical Information

Once the equivalent network has been designed, the next step is to use an electric circuit simulation program to obtain such quantities as the steady state velocity of the particle, the profiles of ionic concentration, the fluid velocity, and so on. We have found PSPICE package most suitable for this purpose. This program is a member of the SPICE family of nonlinear circuit simulators, which can calculate the behavior of analog circuits with high speed and accuracy, even in personal computers. Writing the input file for PSPICE can be done easily if a higher level language is use to produce such a file. The authors can provide any interested reader with a copy of the Pascal routine (only ~90 instructions are needed) that was used in this work. All our analyses were carried out by taking N_c = 300 compartments, enough to ensure good accuracy and moderate CPU times (typically, 2 min, in a PC with a Pentium processor at 200 MHz).

We now explain what information must be obtained from the simulator to get the physical quantities of interest:

(a) Fluid Velocity Distribution. The radial component of the fluid velocity at any point can be obtained by simply knowing the potential at the u_r branch of the circuit (Figures 1d and 2) at each compartment of the system (Figure 3), and using eq 14. In particular, the electrophoretic mobility, μ, can obtained from $u_r(\xi=1)$ using the expression

$$\mu = \frac{(kT)^2 \epsilon_{ext}}{e^2 a \eta} \frac{u_r(\xi=1)}{E_a} \qquad (46)$$

On the other hand, the tangential component of the fluid, v_θ, can be easily obtained from eqs 5 and 9

$$v_\theta(r) = -\frac{1}{2r} \frac{\partial}{\partial r}(r^2 u_r(r)) \qquad (47)$$

(b) Perturbations in Ionic Concentration and Electric Potential. It is also desirable to have information on the profiles of ionic concentrations and electric potential around the particle. Since the angular relationships are given by the cos θ factor in

eq 11, only the variations of either δc_i or $\delta\phi$ with the distance to the particle are of interest. This information can be obtained, as before, by programming PSPICE to output the voltages at all compartments, in the branches corresponding to the different ionic species (Figures 1a, 2, and 3) and to the electric potential (Figures 1b, 2, and 3). With those data, and using expressions 12 and 13, it is easy to obtain the perturbations in concentration and in electric potential.

(c) Modifications Needed To Obtain the Conductivity. Since we are dealing with a heterogeneous system, the effective (or experimentally accessible) conductivity of the suspension, K^*, will relate the average current density, $\langle\vec{I}\rangle$, to the applied electric field $\vec{E}_a$:

$$\langle\vec{I}\rangle = K^*\vec{E}_a \tag{48}$$

We note that the presence of the particles and their charge clouds in an electrolyte solution disturbs the passage of current through the suspension, and therefore K^* will in general be different from the conductivity of the electrolyte solution, K^∞. Nonconducting particles themselves are an obstacle to ionic flows and polarize the incident field, thus altering the bulk conductivity. On the other hand, the diffuse charge cloud surrounding the particles is a region of high conductivity due to the large concentration of counterions, decisively affecting the bulk conductivity of suspension, and allowing K^* to be used in the characterization of the dynamics of the particle's double layer.

In order to perform the conductivity calculations, the following volume-averaged current will be used

$$\langle\vec{I}\rangle = \frac{1}{V}\int_V \vec{I}\,\mathrm{d}V \tag{49}$$

where V denotes a volume containing the particle and its double layer, and it is assumed for the moment that there is a single spherical particle in suspension. In terms of ion fluxes (defined in eq 1)

$$\vec{I} = z_i e N_A \sum_{i=1}^{N}\vec{J}_i \tag{50}$$

By adding and subtracting a term of the form

$$-eN_A\sum_{i=1}^{N}\left(z_i D_i \nabla\delta c_i(\vec{r}) + \frac{z_i^2 e D_i c_i^\infty}{kT}\nabla\delta\phi(\vec{r})\right) \tag{51}$$

the average current becomes

$$\langle\vec{I}\rangle = K^\infty\vec{E}_a + \frac{1}{V}\int_V\left(\vec{I} + \sum_{i=1}^{N} z_i D_i e N_A\left(\nabla\delta c_i(\vec{r}) + \frac{z_i e c_i^\infty}{kT}\nabla\delta\phi(\vec{r})\right)\right)\mathrm{d}V \tag{52}$$

where K^∞, the solution conductivity, is given by

$$K^\infty = \sum_{i=1}^{N}\frac{z_i^2 D_i e^2 N_A c_i^\infty}{kT} \tag{53}$$

We assume a statistically homogeneous suspension[8]

$$\frac{1}{V}\int_V \nabla\delta c_i\,\mathrm{d}V = 0 \tag{54}$$

and make use of the fact that

$$\langle\vec{E}\rangle = -\frac{1}{V}\int_V \nabla(\delta\phi)\,\mathrm{d}V = \vec{E}_a \tag{55}$$

Given that

$$\nabla\cdot\vec{I} = 0 \tag{56}$$

the divergence theorem applied to the volume integral in eq 52 yields

$$\langle\vec{I}\rangle = K^\infty\vec{E}_a + \frac{1}{V}\int_S\left(\vec{r}\,\vec{I}\cdot\mathbf{n} + \sum_{i=1}^{N} z_i D_i e N_A\left(\delta c_i + \frac{z_i e c_i^\infty}{kT}\delta\phi\right)\boldsymbol{n}\right)\mathrm{d}S \tag{57}$$

where S is a (spherical, for simplicity) surface enclosing the particle and its electric double layer and $\boldsymbol{n}$ is the unit vector normal to the surface.

If this surface is far enough from the solid/solution interface, using eqs 1 and 51, $\vec{I}$ can be written

$$\vec{I} = eN_A\sum_{i=1}^{N} z_i D_i c_i^0\nabla\left(\frac{\delta c_i}{c_i^0} + \frac{z_i e\delta\phi}{kT}\right) \tag{58}$$

since $\phi^0 \approx 0$ and $v_r \approx 0$.

Now, taking into account the definition of the functions n_i (eq 3), and substituting (58) into (57), we obtain

$$\langle\vec{I}\rangle = K^\infty\vec{E}_a - \frac{eN_A}{V}\sum_{i=1}^{N} z_i c_i^\infty D_i\int_S(\vec{r}\,\nabla(rn_i)\cdot\mathbf{n} - rn_i\mathbf{n})\,\mathrm{d}S \tag{59}$$

Considering that far from the particle Nernst−Planck equation takes the form

$$\frac{\partial}{\partial r}\left(r^2\frac{\partial rn_i}{\partial r}\right) - rn_i = 0 \tag{60}$$

one has, asymptotically

$$n_i = \left(-\frac{z_i e E_a a}{kT} + \frac{g_i}{r^3}\right) \tag{61}$$

where g_i is a constant that depends on the ionic species considered. Using (61) and (59), and considering already a dilute suspension with N_p particles (i.e., adding N_p integrals like that in (59), all identical)

$$\langle\vec{I}\rangle = K^\infty\vec{E}_a + \Phi\frac{3eN_A}{a^3}\sum_{i=1}^{N} z_i c_i^\infty D_i g_i\frac{\vec{E}_a}{|E_a|} \tag{62}$$

where Φ is the volume fraction of particles, all of which are spheres of radius a. From this equation, the conductivity increment, ΔK, defined by

$$K^* = K^\infty + \Phi\Delta K \tag{63}$$

can be readily calculated.

TABLE 1: Comparison of Simulation Data for the Electrophoretic Mobility (in units of 10^{-8} m^2/(V·s)) with O'Brien and White's[7] Results (O.W.), for Different Values of Zeta Potential and Particle Radius[a]

	$a = 10$ nm		$a = 100$ nm		$a = 1000$ nm	
	O.W.	this work	O.W.	this work	O.W.	this work
$\zeta = 25$ mV	1.2990	1.2995	1.4126	1.4126	1.7937	1.7954
$\zeta = 50$ mV	2.5390	2.5366	2.6297	2.6263	3.4736	3.4709
$\zeta = 75$ mV	3.6610	3.6535	3.5066	3.4989	4.8913	3.8812
$\zeta = 100$ mV	4.6164	4.6027	4.0116	4.0005	5.8844	5.8766
$\zeta = 125$ mV	5.3563	5.3563	4.2281	4.2144	6.3434	6.3313
$\zeta = 150$ mV	5.9132	5.9132	4.2804	4.2655	6.2902	6.2723
$\zeta = 175$ mV	6.3013	6.3013	4.2662	4.2507	5.8801	5.8654
$\zeta = 200$ mV	6.5505	6.5505	4.2382	4.2223	5.3154	5.3102

[a] Values for other parameters of interest are: $z_1 = -z_2 = 1$, $c_1^\infty = c_2^\infty = 10^{-4}$ M, $T = 298$ K, $\epsilon_{ext} = 78.54$, $\epsilon_{int} = 2$, and $\eta = 0.8904$ mPa·s

TABLE 2: Comparison of Simulation Data for the Normalized Conductivity Increment, $\Delta K/K^\infty$, with O'Brien's[8] Results (Ob.), for Different Values of Zeta Potential and Particle Radius[a]

	$a = 10$ nm		$a = 100$ nm		$a = 1000$ nm	
	Ob.	this work	Ob.	this work	Ob.	this work
$\zeta = 25$ mV	5.2729	5.2526	−1.1741	−1.1726	−1.45330	−1.4505
$\zeta = 50$ mV	23.323	23.189	−0.34813	−0.35049	−1.31583	−1.3135
$\zeta = 75$ mV	50.041	49.751	0.71402	0.71033	−1.08582	−1.0842
$\zeta = 100$ mV	81.526	81.044	1.7122	1.7016	−0.77369	−0.77308
$\zeta = 125$ mV	113.44	112.74	2.4647	2.4513	−0.41211	−0.41259
$\zeta = 150$ mV	142.05	141.15	2.9476	2.9327	−0.05131	−0.05112
$\zeta = 175$ mV	165.15	164.09	3.2253	3.2099	0.26292	0.26001
$\zeta = 200$ mV	182.26	181.08	3.3749	3.3590	0.50444	0.50138

[a] Values for other parameters of interest as in Table 1.

(d) Obtention of ΔK from the Circuit Simulation. From eqs 62 and 63, it is readily found that ΔK is known if n_i is determined at a large distance from the particle surface, that is, in the compartments with $\xi \to 0$. This can be done by measuring the voltage at such a node, in the branch corresponding to the Nernst−Planck equations (Figures 1a,b, 2, and 3) and using expressions 61−63. In this work, the distance used from the particle surface has been $\kappa(r-a) = 20$, enough to ensure that the double layer is contained in the volume limited by S, for the values of κ considered.

Results and Discussion

Let us first consider checking the performance and accuracy of the method described, against well-established literature data. Concerning electrophoretic mobility, data in Table 1 allows a comparison with the classical O'Brien and White's results[7] for a wide range of situations. As observed, the agreement between our calculations and the literature results is excellent in all cases, with deviations lower than 1%.

The method works equally well with conductivity calculations, as can be deduced from the comparison between our results and the well-known results of O'Brien,[8] as shown in Table 2.

As we have mentioned, a significant advantage of the method in addition to the fact that the problem of numerical integration is absent (the latter is actually carried out by PSPICE) is that one can readily obtain plenty of information about the steady state of the characteristic quantities of the double layer. In order to illustrate this, we present below some results concerning the perturbations in ionic concentrations, electric potential, and fluid velocity, brought about by the external field, which is assumed to be 1 V/m in all calculations. Given the linearity of the problems in hand, it would suffice to multiply the data presented by the field strength in case that values for $E_a \neq 1$ V/m are needed.

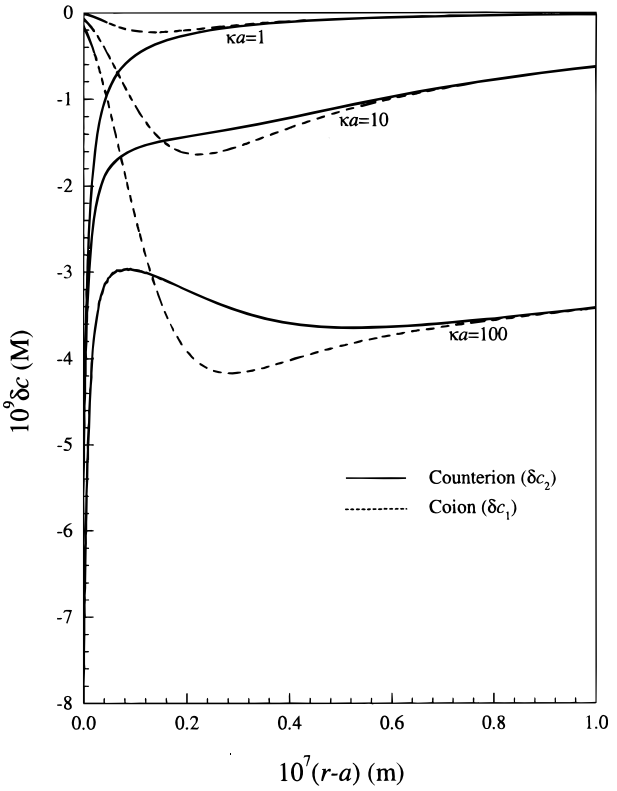

Figure 4. Perturbations in counterion (δc_2) and co-ion (δc_1) concentrations, as a function of the distance to the particle surface, for different values of the dimensionless particle radius, κa. In all curves, $\zeta = 100$ mV, $\kappa^{-1} = 10^{-8}$ m. Applied field: $E_a = 1$ V/m.

Thus, Figures 4−6 show the perturbations δc_1 and δc_2 in the concentration of co-ions and counterions in the direction of the field ($\theta = 0$), as a function of the distance to the particle surface, for different particle sizes, zeta potentials, and counterion valencies, respectively. As expected, whatever the conditions, δc_1 and δc_2 tend to zero far from the particle, and the concentrations of the different ionic species approach its equilibrium value. However, δc_2 is maximum, in absolute value, close to the solid surface; furthermore, the perturbation is negative, due to the balance between two opposed effects: initially, the field will move the (negative) counterions toward the back of the particle (negative contribution to δc_2), but will bring them from the bulk of the solution to the double layer (positive contribution). Furthermore, as soon as the concentrations are perturbed as described, diffusion fluxes will be produced due to the concentration gradients of both co- and counterions. Such fluxes are opposed to those produced by the field, and, for sufficiently large concentration gradients, will be able to exactly compensate the latter, thus bringing about the stationary situation described.

For the case $\zeta = 0$ (Figure 5), δc_2 is positive (although too small to be noticeable in the figure). However, for $\zeta > 0$ the equilibrium double layer must be enriched in counterions, and their tangential flux backward (both electromigrational and diffusive) must be larger than that of counterions coming from the bulk. This explains why δc_2 is more negative the larger the zeta potential (Figure 5). On the other hand, Figure 4 gives us a measure of the characteristic distance to which the perturbation extends out: as mentioned by other authors,[5] the diffusion length of the ions in the polarized double layer is of the order of the

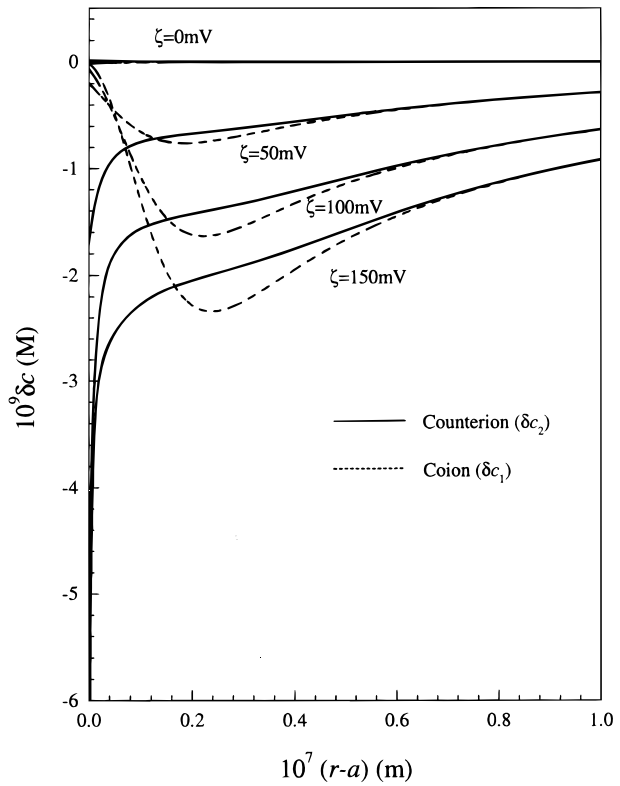

Figure 5. Same as Figure 4, but for different zeta potentials. In all curves, $\kappa a = 10$.

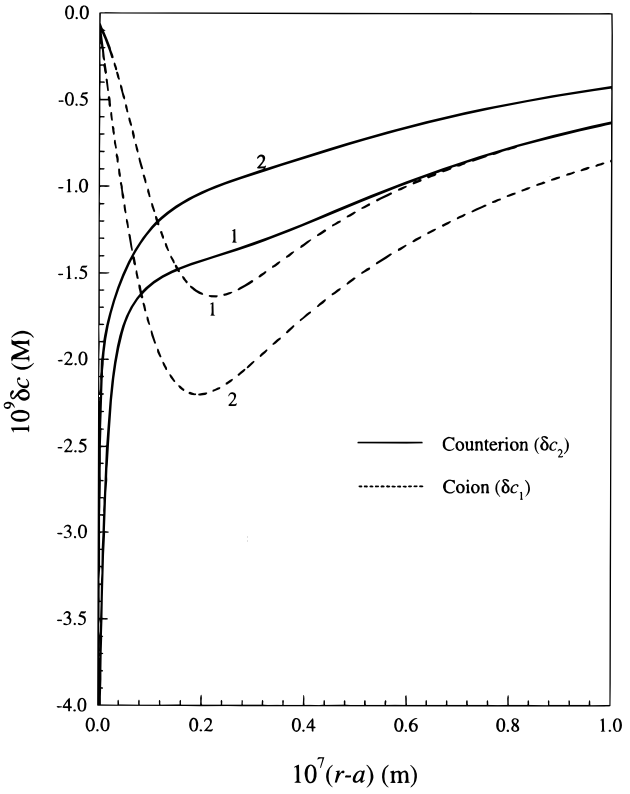

Figure 6. Same as Figure 4, but for different counterion valencies. 1: $z_2 = -1$; 2: $z_2 = -2$. In all curves, $z_1 = 1$, $\zeta = 100$ mV, $\kappa a = 10$.

particle radius. A similar conclusion is reached for the perturbation δc_1 in co-ion concentration (dashed lines). It is worth noting that δc_1 is negative for all zeta values (Figure 5): in this case, (positive) co-ions are moved tangentially by the field to the front of the particle, and normally away from the latter and into the bulk solution. Since, according to the Poisson−Boltzmann equation, the concentration of co-ions in the double layer is very low, the flux of those coming tangentially to the particle front will be lower than that of those being moved into the solution, and hence the negative δc_1 values. Unlike δc_2, the co-ion perturbation first increases in absolute value as we move away from the particle, reaching a maximum and decreasing toward the bulk zero value. As before, the balance between tangential and normal fluxes must be responsible for this fact: close to the particle, the absence of co-ions prevents any fluxes, whereas far from it, equilibrium conditions prevail. In between, the tangential fluxes must increase as the distance raises, since co-ion concentrations are higher the larger the value of $r - a$.

The effect of counterion valency on concentration perturbations is shown in Figure 6 for constant $\kappa a = 10$ and zeta potential $\zeta = 100$ mV. The general trends of variation of both δc_1 and δc_2 with r are similar to those described in Figures 4 and 5. The increase in counterion valency shifts the counterion (co-ion) perturbation upwards (downwards). This shows that a smaller amount of counterions of valency -2 must be moved around the particle in order to achieve the steady state dipole in the double layer, as compared to those of valency -1. Although δc_2 is smaller when $z_2 = -2$, the charge perturbation $z_2\delta c_2$ is larger, as expected. The perturbation in co-ion concentration (δc_1) is larger for $z_2 = -2$ as compared to $z_2 = -1$: the charge perturbation of counterions must be compensated by a larger amount of co-ions, since their valency has not changed. Hence the larger decrease in δc_1 when $z_2 = -2$.

Let us mention, finally, that Figures 4−6 show that both co-ion and counterion concentrations are depleted in the direction of the field (and increased to the same extent for $\theta = \pi$); hence a gradient of neutral electrolyte concentration will be established, a phenomenon known as concentration polarization.[5]

The combined perturbations in δc_1 and δc_2 are shown in Figures 7 and 8, where $\delta\rho = (eN_A(\delta c_1 - \delta c_2))$ (normalized by its value at the particle surface, $\delta\rho_S$) is plotted as a function of $r - a$. We will focus on the effect on such perturbations of changes in particle radius at constant NaCl concentration, and in ionic strength for given particle size. In addition to the expected tendency to zero when $r \gg a$, the main feature of the behavior of $\delta\rho$ is its change of sign for distances of the order of κ^{-1}, already mentioned by other authors,[16,17] but never explained in a fully consistent manner. A qualitative explanation may be offered as follows: the external field will move negative counterions of the double layer toward the left-hand side ($\theta = \pi$) of the particle, thus leaving an excess of positive charge on the right-hand side. This explains the positive values of $\delta\rho$ found in Figures 7 and 8 up to distances of the order of the double layer thickness. On the other hand, the action of the field on anions of the bulk electrolyte will accumulate them close to the double layer limit and provoke the observed negative values of $\delta\rho$ outside the double layer. As mentioned above in connection with our analysis of concentration perturbations, a steady state is reached whereby both electromigration mechanisms are compensated for by diffusive ones, associated with the existence of concentration gradients. Note how for constant κ^{-1} (Figure 7) the distance for which $\delta\rho$ attains zero value is practically the same whatever the particle size, whereas in Figure 8 changes in κ^{-1} bring about corresponding changes in that distance. This seems to confirm our explanation that regions of $\delta\rho > 0$ coincide very approximately with the double layer.

The behavior of the electric potential perturbation ($\delta\phi$), compared to the potential corresponding to the uniform electric

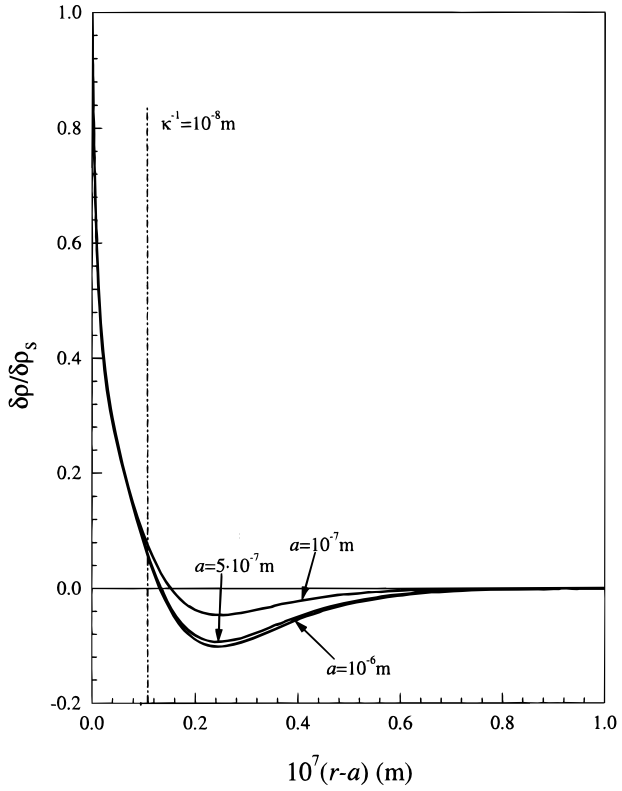

Figure 7. Perturbation in charge density (normalized by surface values, $\delta\rho_S$) as a function of the distance to the particle surface for different particle radii, and constant ζ (100 mV) and ionic strength. Applied field $E_a = 1$ V/m. Approximate κa values: 10 ($a = 10^{-7}$ m), 50 ($a = 5 \times 10^{-7}$ m), 100 ($a = 10^{-6}$ m),

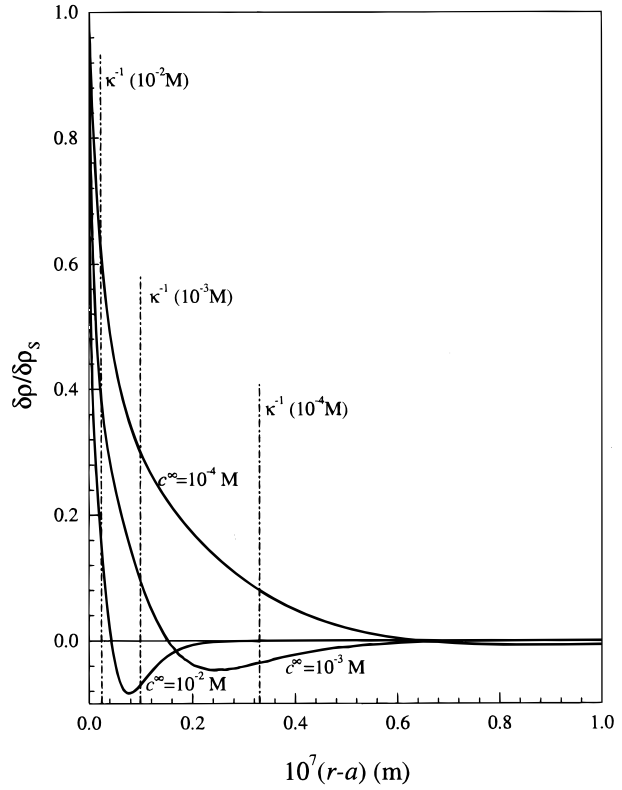

Figure 8. Same as Figure 7, but for different ionic strengths. $a = 10^{-7}$ m; $\kappa a \approx 3$ ($c^\infty = 10^{-4}$ M), $\kappa a \approx 10$ ($c^\infty = 10^{-3}$ M), $\kappa a \approx 30$ ($c^\infty = 10^{-2}$ M).

field, is shown in Figures 9 and 10, as a function of the distance to the particle surface for different values of zeta potential

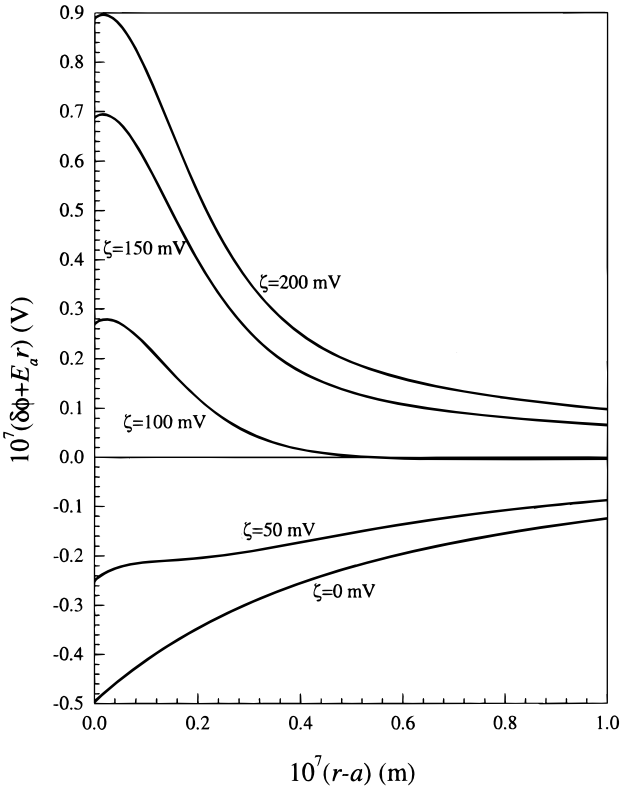

Figure 9. Perturbation in the potential distribution compared to the potential of the external field as a function of the distance to the particle surface for different values of the zeta potential. In all curves $\kappa a = 10$.

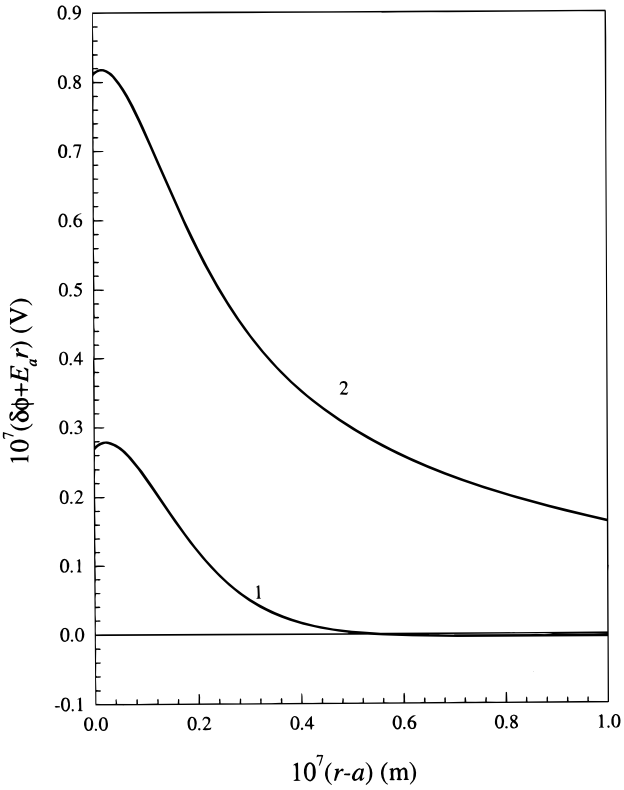

Figure 10. Same as Figure 9, but for different counterion valencies: (1) $z_2 = -1$; (2) $z_2 = -2$. Co-ion valency $z_1 = 1$ in all cases; $\zeta = 100$ mV; $\kappa a = 10$.

(Figure 9) and counterion valencies (Figure 10). As expected, far from the particle, the electric potential tends to the potential corresponding to that of the uniform applied electric field. On the contrary, very strong deviations of $\delta\phi$ appear close to the

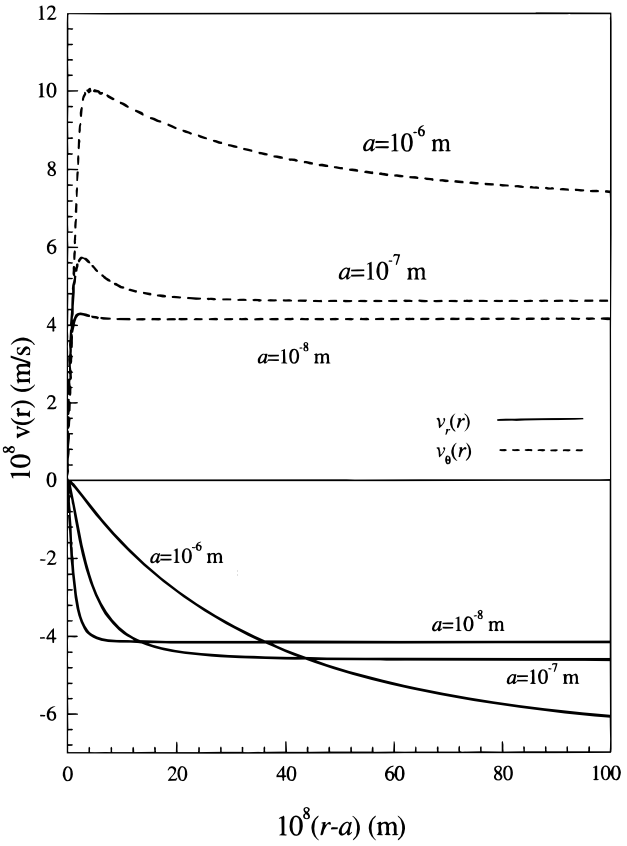

Figure 11. Radial and tangential components of the fluid velocity as a function of the distance to the surface for different values of κa. In all cases, $\zeta = 100$ mV; $\kappa^{-1} = 10^{-8}$ m.

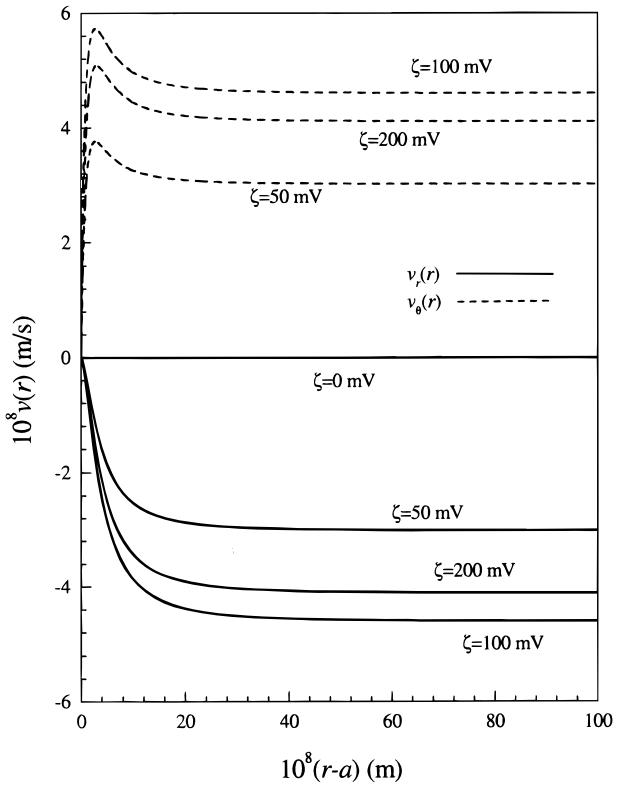

Figure 12. Same as Figure 11, but for different zeta potentials, and $\kappa a = 10$.

solid surface, extending beyond a Debye length from the particle surface. These deviations are larger for larger zeta potentials (Figure 9) and larger counterion valencies (Figure 10). At zero zeta potential, the only effects of the external field would be orientation of the dipoles of both the particle and the aqueous medium, and ion accumulation. Since the dielectric constant of the particle is assumed to be lower that that of the dispersion medium, dipole orientation would give rise to a decrease in potential at the right-hand side of the particle; in addition, cation (anion) accumulation at the left (right) side of the particle should also yield negative $\delta\phi$ values, as observed. When ζ is different from zero, the electric double layer polarization brings $\delta\phi$ toward increasingly positive values (Figure 9), due to the tangential migration of negative counterions toward the left of the particle. Finally, all curves present local maxima for $\zeta \neq 0$, which should be related to the fact that, as shown in Figures 7 and 8, $\delta\rho$ is positive at short distances from the surface.

The effect of increasing the counterion valency on the potential distribution is depicted in Figure 10. As mentioned in reference to Figure 6, a larger dipole is induced in the double layer by the external field, when the counterion valency is increased; this manifests in the increase in potential perturbation for $z_2 = -2$, clearly appreciated in Figure 10.

Another quantity of interest is the fluid velocity distribution around the particle, that is assumed to be the origin of the reference system. Figures 11 and 12 show the radial component of the fluid velocity, v_r, for $\theta = 0$, together with its tangential component v_θ for $\theta = 90°$, as a function of the distance to the surface for different values of a (Figure 11), and different zeta potentials (Figure 12). Note that at large distances from the surface, both tend, in absolute value, to that of the electrophoretic velocity of the particle.

Both figures show that at short distances (comparable to the double layer thickness) to the particle's surface the profiles of the radial and tangential velocities are different: the latter increase with distance much faster that the former, provoked by the electroosmotic flow of liquid due to the motion of negative counterions toward the back of the particle. Figure 11 shows that, at constant zeta potential, increasing the particle radius (for $\kappa a > 1$) brings about a larger particle velocity due to the fact that the surface electric charge increases. Note also that the smaller the particle radius, the smaller the fluid region (of the order of the particle dimensions) that is affected by the presence of the particle and its double layer, a physically meaningful result. This fact, furthermore, explains the crossover of the curves corresponding to different radii. The effect of ζ on both the tangential and radial velocity distributions is plotted in Figure 12. This plot is in agreement with the well-known fact that increasing ζ does not necessarily bring about an increase in velocity, since the braking effect of double layer polarization on particle motion becomes very important at high zeta potentials.

Concluding Remarks

We have shown how the use of a simulation procedure based on the network method allows one to obtain a great amount of information about the perturbed state of the colloidal particle and its double layer, in the presence of a constant external field. The same computation routine used to solve the main problem (for instance, electrophoretic mobility or suspension conductivity) can be employed, without modification, to get that information, since we know the potentials in any branch or node of the electric network used in the simulation. This can be considered one of the main advantages of the methodology described.

Acknowledgment. This work has been supported by the Spanish Ministry of Education and Culture (Projects PB96-0425 and MAT98-0940).

References and Notes

(1) Russel, W. B.; Saville, D. A.; Schowalter, W. R. *Colloidal Dispersions*; Cambridge University Press: London, 1995.

(2) Hunter, R. J. *Zeta Potential in Colloid Science. Principles and Applications*; Academic Press: London, 1981.

(3) Hunter, R. J. *Foundations of Colloid Science*; Oxford University Press: London, 1995; Vol. I.

(4) Lyklema, J. Solid/Liquid Interfaces. In *Fundamentals of Colloid and Interface Science*; Academic Press: London, 1995; Vol. II.

(5) Dukhin, S. S.; Shilov V. N. *Dielectric Phenomena and the Double Layer in Disperse Systems and Polyelectrolytes*; Wiley: New York, 1974.

(6) Wiersema, P. H.; Loeb, A. L.; Overbeek, J. Th. G. *J. Colloid Interface Sci.* **1966**, 70.

(7) O'Brien, R. W.; White, L. R. *J. Chem. Soc., Faraday Trans. 2* **1978**, *74*, 1607.

(8) O'Brien, R. W. *J. Colloid Interface Sci.* **1981**, *81*, 234.

(9) Oster, G. F.; Perelson; Katchalsky. *Nature* **1971**, *234*, 393.

(10) Oster, G. F.; Perelson; Katchalsky. *Q. Rev. Biophys.* **1973**, *6*, 1.

(11) Horno, J.; Castilla, J.; González-Fernández, C. F. *J. Phys. Chem.* **1992**, *96*, 854.

(12) Moya, A. A.; Castilla, J.; Horno, J. *J. Phys. Chem.* **1995**, *99*, 1292.

(13) Horno, J.; García-Hernández, M. T.; González-Fernández, C. F. *J. Electroanal. Chem.* **1993**, *352*, 83.

(14) Horno, J.; García-Hernández, M. T.; González-Fernández, C. F. *J. Electroanal. Chem.* **1994**, *377*, 53.

(15) López-García, J. J.; Moya, A. A.; Horno, J.; Delgado, A.; González-Caballero, F. *J. Colloid Interface Sci.* **1996**, *183*, 124.

(16) Grosse, C.; Foster, K. R. *J. Phys. Chem.* **1987**, *91*, 3073.

(17) Pedrosa, S.; Grosse, C. *Anal. AFA* **1996**, *8*, 254.